



## Article

# Mapping Small-Scale Willow Crops and Their Health Status Using Sentinel-2 Images in Complex Agricultural Areas

Hadi Beygi Heidarlou <sup>1,2</sup>, Octavian Oprea-Sorescu <sup>1</sup>, Marina Viorela Marcu <sup>1</sup> and Stelian Alexandru Borz <sup>1,\*</sup>

<sup>1</sup> Department of Forest Engineering, Forest Management Planning and Terrestrial Measurements, Faculty of Silviculture and Forest Engineering, Transilvania University of Braşov, Şirul Beethoven 1, 500123 Braşov, Romania; h.beygi@urmia.ac.ir (H.B.H.); opreasoarescuoctavian@yahoo.com (O.O.-S.); viorela.marcu@unitbv.ro (M.V.M.)

<sup>2</sup> Forestry Department, Faculty of Natural Resources, Urmia University, Urmia P.O. Box 165, Iran

\* Correspondence: stelian.borz@unitbv.ro; Tel.: +40-742-042-455

**Abstract:** The goal of this study was to estimate the areas under willow cultivation by farmers, as well as their growth and health status. Due to the extremely small patch size of land cover types in the study area, Sentinel-2 data were used to conduct supervised classification based on the random forest machine learning technique, and a large training dataset was produced from PlanetScope satellite imagery. The results of image classification using Google Earth Engine indicated that the Sentinel data were suitable for identifying willow-cultivated areas. It was found that these areas declined from 875.32 ha in 2017 to 288.41 ha in 2022. The analysis of the growth and health conditions of willow-cultivated plots also revealed that the temporal variations in the NDVI in these plots decreased significantly in 2022 as compared to previous years ( $p < 0.05$ ). An in-depth analysis revealed a significant positive correlation between NDVI, precipitation, and temperature. It was found that the most efficient components explaining the process of browning the vegetation in the planted willow plots were the increasing temperature and decreasing precipitation. This research may be used to document the national and global monitoring efforts for climate change adaptation.

**Keywords:** dot-grid approach; Google Earth Engine; NDVI variations; PlanetScope; random forest; willow short-rotation crops



**Citation:** Beygi Heidarlou, H.; Oprea-Sorescu, O.; Marcu, M.V.; Borz, S.A. Mapping Small-Scale Willow Crops and Their Health Status Using Sentinel-2 Images in Complex Agricultural Areas. *Remote Sens.* **2024**, *16*, 595. <https://doi.org/10.3390/rs16030595>

Academic Editor: Dino Ienco

Received: 10 January 2024

Revised: 1 February 2024

Accepted: 2 February 2024

Published: 5 February 2024



**Copyright:** © 2024 by the authors. Licensee MDPI, Basel, Switzerland. This article is an open access article distributed under the terms and conditions of the Creative Commons Attribution (CC BY) license (<https://creativecommons.org/licenses/by/4.0/>).

## 1. Introduction

Concerns about climate change, energy supply, growing greenhouse gas emissions, and rising fossil fuel price have driven a significant effort in searching for clean and renewable conventional fuel alternatives in recent years [1]. Bioenergy is one of the most important resources available to help meet humanity's energy demands and replace fossil fuels, and interest in it has grown sharply in recent years [2]. Biomass is defined as any organic substance that has absorbed sunlight and stored it as chemical energy, such as wood, wood waste, straw, manure, sugar cane, and many other agricultural byproducts [3]. Therefore, energy from biomass is a very flexible energy source that can be rapidly scaled to meet the demand, and as a result, it is a perfect complement to weather-dependent renewable sources such as wind and solar energy.

Considering the European Union's most significant aim of reducing greenhouse gas emissions by a quarter and increasing energy efficiency and the use of renewable energy [4], Romanian entrepreneurs have started to test and implement bioenergy projects, most of which are based on the provision of fuels from short-rotation crops, including willow (*Salix* spp.). Willow short-rotation crops (SRCs) have been tested and used to source renewable raw materials for bioenergy production since 2008 [5]. Currently, they are an important renewable energy source that is mostly turned into thermal energy utilizing biomass processing technology; willow SRCs have contributed to the European Union's

renewable energy objectives since they are a cost-effective choice for locations with large untapped biomass production potential [6].

Monitoring crop condition, phenology, and changes in land cover and land use and allocating agricultural land to these crops [7,8] provide critical information for the development and implementation of sustainable energy management policies and the reduction in greenhouse gas emissions. While systematic and open-source remote sensing provides a wealth of data and imagery with high spatial and temporal resolutions on land-use change and bioenergy use [9], what happens to the land once it is allocated to these activities differs by region [10]. This has opened up the possibility of conducting complete bioenergy and biomass production studies over a longer time frame using multi-source remote sensing data. In addition, there is no worldwide product that gives information useful for the local classification of land use for bioenergy purposes.

There are several ways for estimating and evaluating the condition and the area of various land cover types. These approaches range from agricultural national census to other forms of remote sensing and GIS techniques. For area estimates, the most often-used approach is wall-to-wall or sample-based mapping [11–14]. However, landscape classification might be problematic nowadays because the average plot size has been decreasing. Also, acquiring multi-source feature sets with high quality is difficult due to diverse imaging techniques and spatiotemporal resolution [15,16]. In Southeast Asia, for example, the average size of agricultural fields declined from 2.5 hectares to 1 hectare between 1950 and 2000 due to farm fragmentation caused by population expansion [17]. To overcome these challenges, a combination of medium spatial resolution satellite images, such as those provided by the European Space Agency (ESA) Sentinel-2 (with a spatial resolution of 10 m), with high spatial resolution satellite images, such as those provided by PlanetScope satellites (with a higher spatial resolution of 3 m), can be used. This combination, which uses various spectral bands, increases the capacity to discern land cover types and agricultural crops and allows the human eye to distinguish characteristics better. As a result, the object-based classification algorithms used provide a precise representation of land surface classification [18].

The calculation and use of vegetation indices (VIs) generated from remote sensing imagery is a typical strategy in examining the condition and health of vegetation covers for both agricultural crops and forests [19]. In particular, VIs have been developed to assess a wide range of environmental and biological events [20,21] and may be used to forecast plants' biophysical characteristics [22]. Climate change, land-use change, and natural disturbances such as wildfires and insect outbreaks can all have an impact on vegetation greening and browning patterns [23–25], while VIs estimated from the red and near-infrared (NIR) bands are still commonly used in this context [26]. The normalized difference vegetation index (NDVI) [27] is commonly used to quantify vegetation changes and to study the effects of environmental events. Several studies have used the NDVI to characterize vegetation phenology [28,29] and to classify land cover [30,31], while the NDVI has been used in a wide range of applications in ecology, economics, agriculture, drought monitoring, and in characterizing climatic effects on plants [32,33].

As a result of the development of all of these instruments and indicators, researchers and governmental and international organizations and institutions have used these data to study adverse environmental occurrences, vegetation conditions, and even the performance of agricultural products [34]. Several years of work in this field have demonstrated that the use of satellite data, the combination of spectral bands in the identification of land uses and land covers, and the use of vegetation indices (such as the NDVI), have great potential in determining how external and environmental factors affect vegetation [35]. These technologies have the potential to detect various agricultural products, tree plantations and their health status, and material shortages induced by weather.

Despite the fact that the cultivation of willow (*Salix* spp.) for bioenergy purposes has been performed in Romania for the last 15 years (since 2008), there are no publicly available aggregated statistics on their condition, location, and size. Partly, this comes from the fact

that such crops were typically established on small-sized areas, in dispersed locations [36], at a well-sustained pace, making it difficult to keep track of them, monitor their condition, and formulate and implement governmental bioenergy policies. The situation is similar to other European countries, for which the characterization of such crops typically relies on several data sources [37]. As a result, the main goal of this study was to check if the combined use of medium- and high-resolution satellite images can help in detecting and classifying the agricultural plots under willow SRC production. On the other hand, field observations and time series extracted from satellite images may give evidence of variations in terrestrial vegetation activity by detecting greening and browning cycles in plants throughout time. As a second goal, this study looked at the NDVI trend changes in planted willow plots for more detailed monitoring of vegetation conditions. Consequently, the following were the objectives of this research: (1) detecting changes in the willow SRC planting areas, and (2) tracking their growth and health status.

By using this research approach in Eastern Europe and Central Romania as an example, we propose a simple, cost-effective, strategic, and transparent technique for mapping small crops of willows in areas dominated by a mix of complex peri-urban agriculture and forest environments. Understanding the distribution of planted willow plots and land covers in the study area provides a good overview of the development of willow SRC production in the entire region using the Google Earth Engine (GEE) platform and Sentinel-2 time-series images from 2017 to 2022, as cultivation patterns are generally similar. However, the approach may be used in other regions of the world where changes in landscape and land use/cover are frequent.

## 2. Materials and Methods

### 2.1. Study Area

The area of study was selected in the central part of Romania, in Braşov and Covasna counties, for which there was evidence of established willow crops. As a fact, location data were available for several plots from a study carried out by the last two authors with the aim to evaluate the productivity of willow planting operations [36]. Also, expert information was obtained from a grower within the area, pointing the selection of the study area to the possible extents of areas cultivated with willows in the region. As a third criterion, the area was selected so as to maximize the coverage of some satellite datasets which were provided on request to the first author of the study.

The study area covered 137,137 ha, being located in between  $45^{\circ}38'27.63''N$  to  $46^{\circ}2'5.229''N$  and  $25^{\circ}45'11.193''E$  to  $26^{\circ}13'0.841''E$ , respectively (Figure 1); it is an intramountainous depression characterized by a moist-temperate climate with strong continentalism. Generally, the weather is colder compared to the surrounding regions.

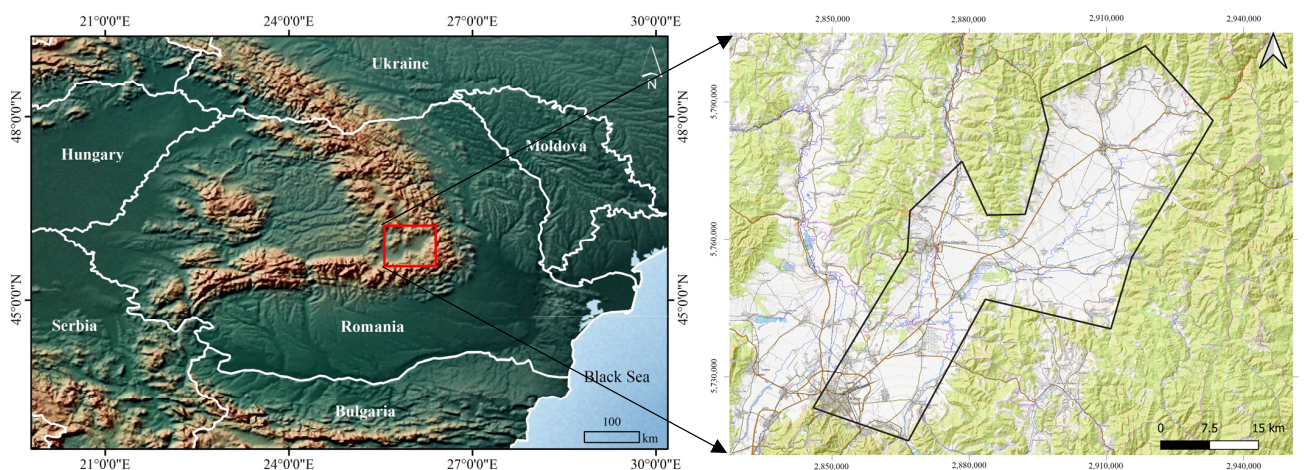


Figure 1. Geographical location of study area.

## 2.2. Datasets

### 2.2.1. Satellite Images for Classification

All Sentinel-2 bands with 10 and 20 m spatial resolution, including blue (B2); green (B3); red (B4); red-edge 1, 2, and 3 (B5, B6, and B7); near-infrared (NIR, B8); SWIR 1; and 2 (B11 and B12), for the region were obtained in GEE as image collections from February to August (2017 to 2022), which corresponds to the months when willows grow in the study area. Bands B2, B3, B4, and B8, which had a resolution of 10 m, were extensively used for image classification. The chlorophyll content of the crops was well represented by the B5 to B7 bands [38,39]. B11 and B12 bands were connected to the water content of plants and crops [40,41]. It has been established that these bands can distinguish between different types of agricultural crops [42]. Sentinel-2 surface reflectance products that had a cloud cover of less than 5% were used for all time points (2017 to 2022) (Table 1). This was made feasible by the fact that during the study period, most of the region had clear images.

**Table 1.** Details of satellite images used for classification.

Year	Image Collection	Sensor	Number of Images
2022			27
2021			26
2020	COPERNICUS/S2_SR	Sentinel-2	29
2019			18
2018			26
2017			10

### 2.2.2. Ground Reference Data

Extensive fieldwork and high-resolution Google Map satellite imagery were used to collect reference data for training and validation in 2022. The borders of all willow-planted plots found by the field survey were taken using GPS in 2022 and integrated into the available willow-plot dataset. According to the primary goal of this study, the data were collected according to two classes of land use: willow and non-willow areas (e.g., agricultural lands, forest, residential areas, water bodies, etc.). Willow crops and other different types of agricultural plots in the region were visited from February to August 2022 in order to understand the land-use types.

For the years before 2022, PlanetScope satellite imagery [43] was used to identify the willow plots. Planet, one of the most prominent private earth imaging companies, presently operates more than 200 PlanetScope satellites capable of mapping the entire earth's land surface virtually every day [44]. PlanetScope images calibrated to the top of atmospheric radiance and with four spectral bands, including R.G.B. and NIR, were used in this study for the period of 2017 to 2021, with a 3 m ground sample distance [44]. These images have been accessible for the study area since 2016. Figure 2 shows an example of reference data collected for willow plots in 2018.

Procedurally, the reference data were collected from Google satellite and PlanetScope images using the dot-grid photo interpretation technique [45,46]. Absence of subjectivity, the methodical approach, and quick sample collection are some benefits of the dot-grid approach [47]. In order to have a balanced distribution of points over the whole region and to provide reference data for the non-willow class, square cells with an area of 2 square kilometers (km<sup>2</sup>) were created at intervals of 5 km (from the cell center). The dots were then systematically created at 7 m intervals inside these cells and willow plots at random (Figure 3). In addition, we avoided gathering samples of various classes (i.e., willow and non-willow) which were too close to each other in order to avoid mixed samples within 20 × 20 m areas by building 20 m buffers inside and outside the willow plots. If the willow plot was found inside the 2 km<sup>2</sup> cells, the dots that were placed on it were considered as willow class.

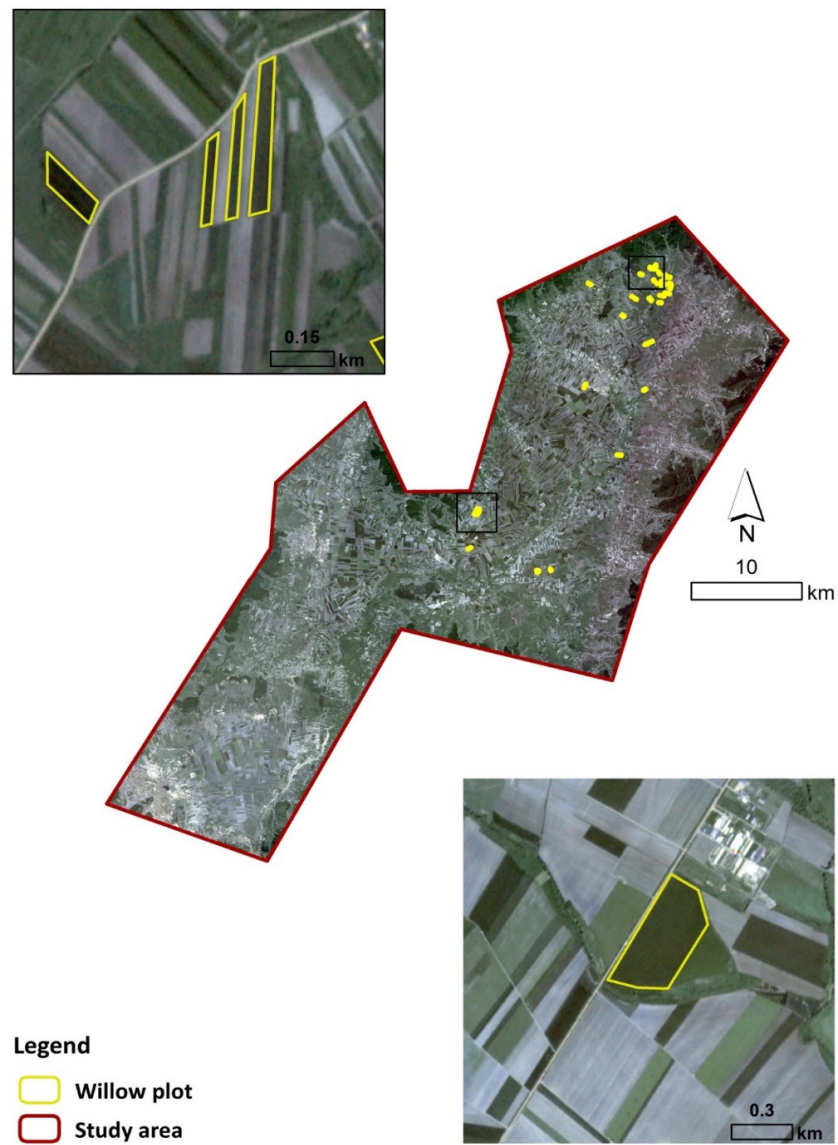


Figure 2. Example of reference data collected for willow plots in 2018 using PlanetScope satellite imagery.

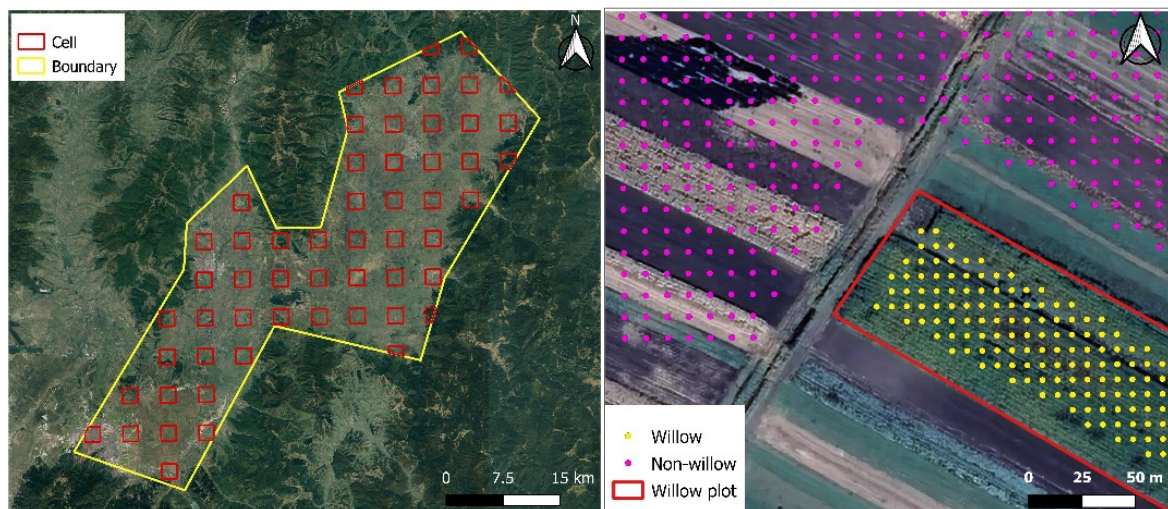


Figure 3. An example of generated reference data.

Table 2 lists the characteristics of the multi-temporal reference datasets for the studied years. The subsets for training (50%) and validation (50%) were randomly selected from the reference datasets.

**Table 2.** The characteristics of the multi-temporal reference datasets.

Land-Use Class	Definition	Total Number of Reference Points (at 7 m Intervals)					
		2017	2018	2019	2020	2021	2022
Willow	Willow crops	6431	4127	5967	6043	6929	7022
Non-willow	Other land uses <sup>1</sup>	7661	7662	7664	7654	7656	7666

<sup>1</sup> Croplands, built-up areas, forests, and other natural areas are all included.

### 2.3. Image Classification

To effectively identify the willow and non-willow classes, the GEE cloud computing platform was used to provide image collections, preprocess, extract features, classify, and check the accuracy of produced maps [48]. This stage entailed a number of procedures, including image collecting and filtering, cloud-cover masking, calculation of spectral indices, extraction of spectral-temporal information, and classification [49,50]. For image classification and the training samples, a nonparametric random forest (RF) classifier was used. Using this method in the GEE cloud platform, 70% of the sample data were randomly picked for classifier training and image classification, while the remaining 30% were used for verifying and evaluating classification results. Multi-classifier (tree-type) ensemble techniques are used in RF classification [50]. Regarding the hyperparameter tuning, only the number of trees (ntree) and the number of predictors (mtry) were tuned, and for the rest, the default values were used. Hyperparameter tuning was based on the earliest dataset (2022), and the optimal values (ntree = 500, mtry = 10) were used to generate land-use maps for the rest of the datasets. Sentinel-2 surface reflectance products (from 2017 to 2022) were used for this purpose in this study.

Several studies [47,51–54] have shown that spectral bands are critical for classification and that using more spectral bands enhances the accuracy for applications like crop mapping up to a certain threshold. As a result, spectral vegetation indices (SVIs) and all bands from Sentinel-2 images were used in GEE classification algorithms. The NDVI (normalized difference vegetation index), std NDVI (standard deviation of NDVI), GNDVI (green normalized difference vegetation index), MSAVI (modified soil-adjusted vegetation index), and EVI (enhanced vegetation index) are five vegetation indices (Table 3) that are often used in studies [55].

**Table 3.** Spectral vegetation indices (SVIs) used for detecting willow crops.

SVI <sup>1</sup>	Definition	Formula	Reference
NDVI	Normalized difference vegetation index	$(B_{NIR} - B_{RED}) / (B_{NIR} + B_{RED})$	[56]
std NDVI	Standard deviation of NDVI	$\sigma_{NDVI}$	[57]
GNDVI	Green normalized difference vegetation index	$(B_{NIR} - B_{GREEN}) / (B_{NIR} + B_{GREEN})$	[58]
MSAVI	Modified soil-adjusted vegetation index	$\frac{2B_{NIR} + 1 - \sqrt{(2B_{NIR} + 1)^2 - 8(B_{NIR} - B_{RED})}}{2}$	[59]
EVI	Enhanced vegetation index	$2.5 \times \frac{B_{NIR} - B_{RED}}{1 + B_{NIR} + 6 \times B_{RED} - 7.5 \times B_{BLUE}}$	[60]

<sup>1</sup> SVI: spectral vegetation index.

The spectral-temporal metrics (STMs) were derived using per-pixel statistics, such as minimum, maximum, mean, standard deviation, and 25th, 50th, and 75th percentiles (Table 4). In addition to STMs, elevation data from the Shuttle Radar Topography Mission (SRTM) were used to create elevation and slope layers [61].

**Table 4.** Multi-temporal satellite images and STMs used for image classification.

Time Period	Mission	No. of Images	STMs	No. of Features
2017 to 2022	Sentinel-2	136	Minimum, maximum, mean, standard deviation, and 25th, 50th, and 75th percentiles	119

#### 2.4. Post-Classification Processing

A  $3 \times 3$  kernel-size filter with the majority vote was applied to eliminate misclassification effects in the classified images [62]. An accuracy assessment was used to evaluate the performance of the willow/non-willow classified maps by randomly selecting 50% of the reference data. The overall accuracy ( $OA$ ) (Equation (1)), kappa coefficient ( $K$ ) (Equation (2)), producer's accuracy ( $PA$ ) (Equation (3)), user's accuracy ( $UA$ ) (Equation (4)), and  $F$ -score ( $F$ ) (Equation (5)) were chosen in this study since these are often used in the field of remote sensing to assess classification quality. The  $OA$  represents the proportion of pixels that were successfully classified, with 85% or above being recognized as a satisfactory classification threshold. The  $PA$  represents map accuracy from the map producer's perspective. It indicates how frequently features on the ground are accurately depicted on the classified map [63]. The  $UA$  is the accuracy from the perspective of a map user. It specifies how frequently the features listed on the map will be present on the ground [64].  $K$  measures the degree of agreement between classifier output and reference data [65].  $F$  is a per-class metric computed as the harmonic mean of the user's and producer's accuracies [66].

$$OA = \frac{\sum_{i=1}^r X_{ii}}{N} \quad (1)$$

$$K = \frac{N \sum_{i=1}^r X_{ii} - \sum_{i=1}^r (X_{i+} \times X_{+i})}{N^2 - \sum_{i=1}^r (X_{i+} \times X_{+i})} \quad (2)$$

$$PA\% = \frac{\text{Number of correctly classified pixels of a particular class}}{\text{Number of reference pixels of the same class}} \times 100 \quad (3)$$

$$UA\% = \frac{\text{Number of correctly classified pixels of a particular class}}{\text{Number of classified pixels in the class}} \times 100 \quad (4)$$

$$F = 2 \times \frac{PA \times UA}{PA + UA} \quad (5)$$

where  $r$  represents the number of rows in the confusion matrix,  $X_{ii}$  represents the number of observations in row  $i$  and column  $i$ ,  $X_{i+}$  represents the total number of observations in row  $i$ ,  $X_{+i}$  represents the total number of observations in column  $i$ , and  $N$  represents the total number of observations in the matrix.

#### 2.5. NDVI Time Series

The NDVI is often used in modern specialized studies of changes and inter-annual fluctuations in the quality of ecosystems, vegetation, or crops in general [67,68]. Also, the NDVI is used in locations across the world where vegetation is vulnerable to changes in extreme climatic conditions (thermal stress, lack of moisture, and decreasing rainfall) [69,70]. Sentinel-2 satellite data were used to generate NDVI time series (derived from the B4 and B8 bands [58]) for willow crops in the studied area at a spatial resolution of 10 m in order to quantify vegetation greenness (changes in plant health) [71]. The Sentinel-2 satellite provides time-series global vegetation indices with an average revisit period of 5 days and a spatial resolution of 10 m [72].

The GEE cloud computing platform was used to combine Sentinel-2 ('COPERNICUS/S2\_SR') vegetation index data from April 2017 to December 2022 to create a dense NDVI time series with a temporal resolution of approximately 2 days. Annual and monthly NDVI layers were generated using two filters: (1) choosing images with less than 20% cloud cover and (2) selecting soil or vegetation pixels in the previously chosen images. The Scene

Classification Layer (SCL) provided with Sentinel-2 data was used for this purpose [73]. In addition, the Sentinel-2 QA [74] band or cloud scoring algorithm [75] was used to develop a cloud-masking filter [76]. Then, seasonal NDVI time series for willow plots were created using Sentinel-2 images from April 2017 to December 2022. In order to avoid obtaining NDVI values for other land uses near the willow plots, a 20 m buffer was created inside the willow plots. As a result, the 10 willow plots planted since 2017 with the largest area were chosen for NDVI calculations following the detection of willow plots through image classification. The NDVI of the willow plots was calculated by averaging the NDVI data of these plots.

## 2.6. Climate Datasets

Over the study period (2017–2022), daily temperature and precipitation measurements were collected from the Sfântu Gheorghe weather station, which belongs to the Romanian National Meteorological Administration and is located in the depression of Sfântu Gheorghe, which occupies the central-north part of the Brasov Depression, one of the largest in the Carpathian Mountains.

## 2.7. Statistical Analysis

The average monthly and annual temperatures, precipitation, and NDVI changes in the study area were evaluated using one-way analysis of variance (ANOVA). Additionally, Duncan's test was applied to compare the average of the investigated indicators across various years and months. The correlation coefficient method was used to assess the relationship between NDVI and meteorological parameters (such as temperature and precipitation). This relationship was computed as follows:

$$r = \frac{\sum_{i=1}^n (x_i - \bar{x})(NDVI_i - \overline{NDVI})}{\sqrt{\sum_{i=1}^n (x_i - \bar{x})^2} \sqrt{\sum_{i=1}^n (NDVI_i - \overline{NDVI})^2}} \quad (6)$$

where  $n$  is the number of observations,  $i$  is the time,  $x_i$  is the climatic factor value, and  $NDVI_i$  is the NDVI value. This study used three levels of correlation coefficients: strong correlation ( $\pm 0.8 < r \leq \pm 1$ ), moderate correlation ( $\pm 0.3 < r \leq \pm 0.8$ ), and insignificant correlation ( $0 < r \leq \pm 0.3$ ).

## 3. Results

### 3.1. RF Classification Accuracy

The capacity of Sentinel-2 multi-temporal images to detect and map willow crops with different feature sets using RF was evaluated here. Using the reference samples from Google Maps and PlanetScope satellite imagery as training data for the RF classifier in GEE, Sentinel-2 data were able to classify willow/non-willow plots in the study area at OA rates of 98% and higher for all of the six images produced for the period of 2017 to 2022 (Table 5 and Figure 4). These values reflect the percentage of the territory that has been effectively classified as willow and non-willow for all time periods. Per-class accuracy rates were also consistently high, with values over 98% for the UA, PA, and F metrics.

**Table 5.** Accuracy metrics by different input data feature sets.

Class	2017			2018			2019		
	UA <sup>1</sup>	PA <sup>2</sup>	F <sup>3</sup>	UA	PA	F	UA	PA	F
Willow	99.10	98.63	98.86	99.76	99.03	99.39	99.37	99.21	99.29
Non-willow	99.48	99.87	99.67	99.41	99.53	99.47	99.48	99.87	99.67
OA <sup>4</sup>		98.98			99.57			99.39	
K <sup>5</sup>		97.93			99.07			98.76	

Table 5. Cont.

Class	2020			2021			2022		
	UA	PA	F	UA	PA	F	UA	PA	F
Willow	99.67	98.71	99.19	99.70	99.01	99.35	99.76	99.63	99.74
Non-willow	98.95	99.74	99.34	99.14	99.74	99.44	99.65	99.78	99.75
OA		99.27			99.40			99.71	
K		98.53			98.79			99.41	

<sup>1</sup> UA—user accuracy (%), <sup>2</sup> PA—producer accuracy (%), <sup>3</sup> F—F-score (%), <sup>4</sup> OA—overall accuracy (%), <sup>5</sup> K—Kappa coefficient.

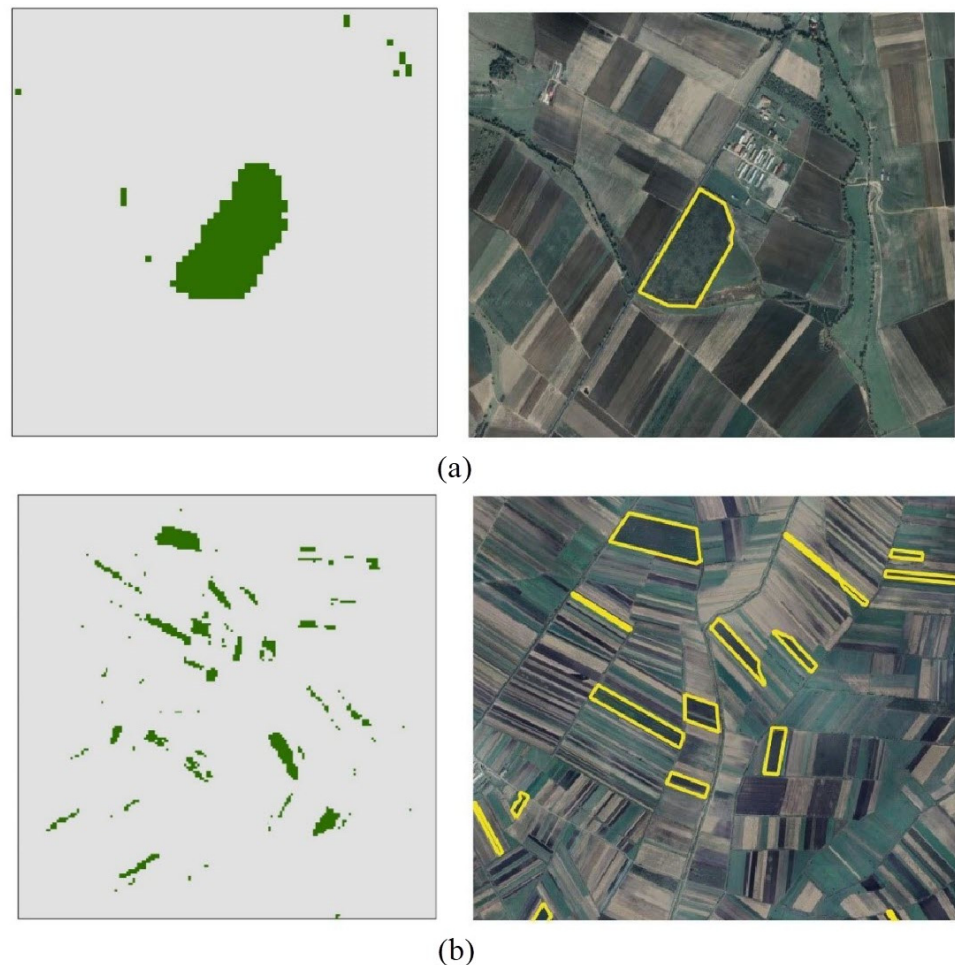


**Figure 4.** Classification findings from Sentinel-2 for two study area parts (a) in 2022 with Google Maps satellite imagery in QGIS on the right, and (b) in 2018 with PlanetScope images on the right. (The yellow polygons represent the boundary of willow-planted plots).

### 3.2. RF Classification Results

Willow planting patterns and inconsistencies with respect to yearly differences were examined from 2016 to 2022. Figures 5 and 6 show the spatial patterns associated with the willow and non-willow classes by the maps developed for the study area. As predicted by the method, willow plots covered 0.64% of the area in 2017, but they declined to 0.21% in 2022. On the other hand, the non-willow lands increased from 99.36% to 99.79% during the same time period. As shown in Figure 6, farmers planted most of the willows in 2016, and after that the area cultivated has declined. In addition, the northern part of the region was characterized by an increased interest in willow planting over these years.

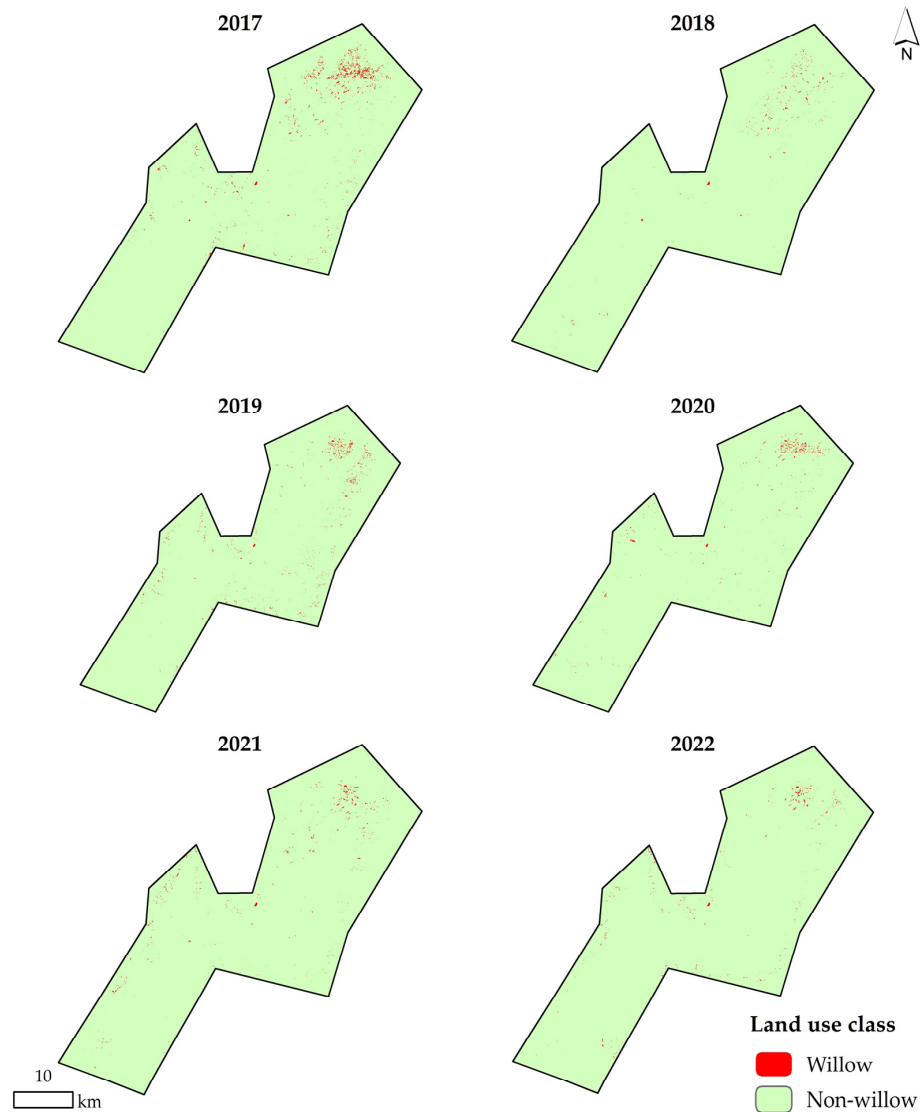


Figure 5. Land-use classification results of the study area using Sentinel-2 images.

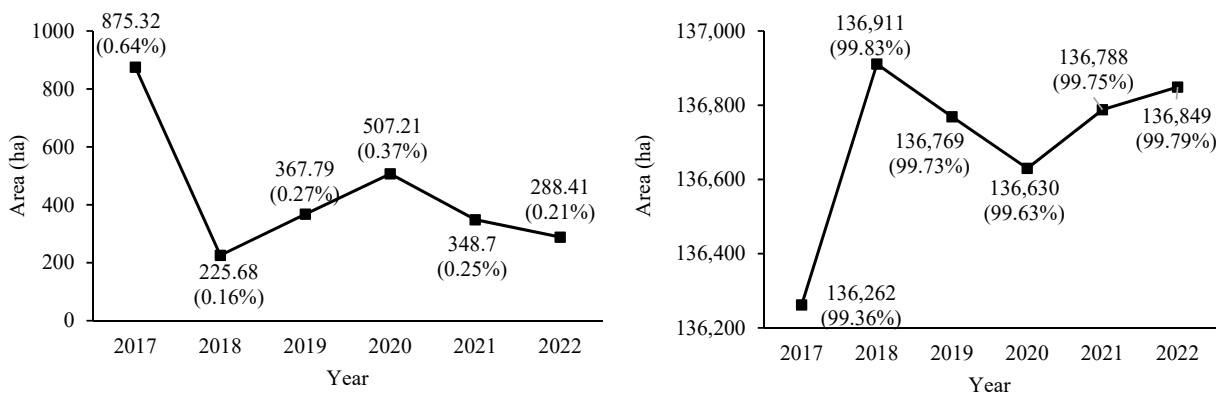
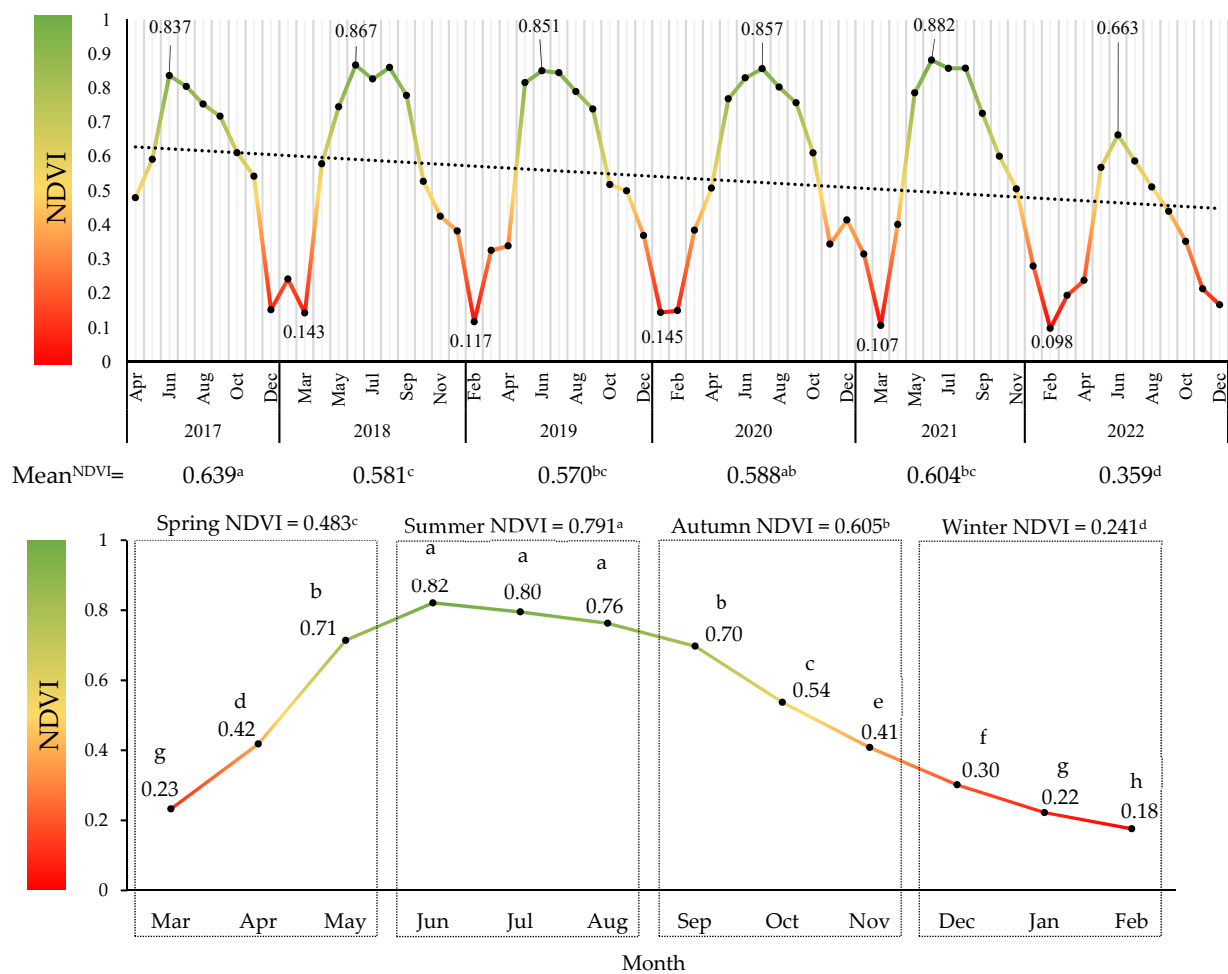


Figure 6. Area of the willow (left) and non-willow (right) classes in the period of 2017–2022.

### 3.3. NDVI Inter-Annual Fluctuation

According to the crop calendar, the resulting NDVI time series reveal a specific phenological peak connected to willow crop growth. From 2017 to 2022, the mean NDVI value in the willow plots had distinct features (Figure 7). The multi-year average value of the

NDVI was 0.557, with the lowest value of 0.098 in February 2022 and the maximum value of 0.882 in June 2021. Every year, the NDVI fluctuated, with the highest values appearing in summer (from June to August) and the lowest values appearing from December to March. When compared to other months of the year, June, July, and August had the highest NDVI values, according to Duncan’s test, and these differences were significant (at the 5% level). The NDVI also reached its lowest point in February. The monthly average value of the NDVI reached 0.82 in June, and willow growth was typically good, but the monthly average value of the NDVI reached 0.18 in February, and willow growth was limited owing to the winter season, fall leaves, and occasionally even yearly harvests. The NDVI value in the region was relatively high from June to August, which is often considered the willow growing season. The NDVI range in the area remained vast and constant from 2017 to 2021 (min  $\approx$  0.1, max  $\approx$  0.8); however, the peak value of the NDVI in 2022 was reduced from about 0.9 in prior years to 0.663. The average yearly NDVI values also revealed that the value of this index in 2022 was 0.359, a substantial variation from prior years.



**Figure 7.** Changes in NDVI in the study area from 2017 to 2022: yearly average scale (**top**) and seasonal and monthly average scale (**bottom**). (Different letters indicate statistically significant differences ( $p \leq 0.05$ )).

At the 5% probability level, the results from ANOVA revealed a statistically significant difference between the seasonal, annual, and monthly NDVI values (Table 6). Figure 7 shows that 2017 and the summer season had the highest annual and seasonal average NDVI values, respectively, while 2022 and the winter season had the lowest.

**Table 6.** ANOVA results for NDVI values.

		Sum of Squares	df	Mean Square	F	Sig.
Yearly	Between Groups	26.067	5	5.213	92.518	0.000
	Within Groups	126.956	2253	0.056		
	Total	153.023	2258			
Monthly	Between Groups	102.18	11	9.289	410.537	0.000
	Within Groups	50.842	2247	0.023		
	Total	153.023	2258			
Seasonal	Between Groups	71.523	3	23.841	659.645	0.000
	Within Groups	81.5	2255	0.036		
	Total	153.023	2258			

**3.4. Climatic Variable Changes**

By comparing the mean precipitation from 2017 to 2022, it was found that the amount of monthly precipitation in June, which represents the start of the peak growth season of vegetation, was reduced significantly in 2022 (at the 5% level) (Figure 8). The highest amount of precipitation was in June 2018, following which a downward trend was found. In the studied time period (2017–2022), there were no significant changes in the daily amount of precipitation in other months of the vegetation growth period (May to September).

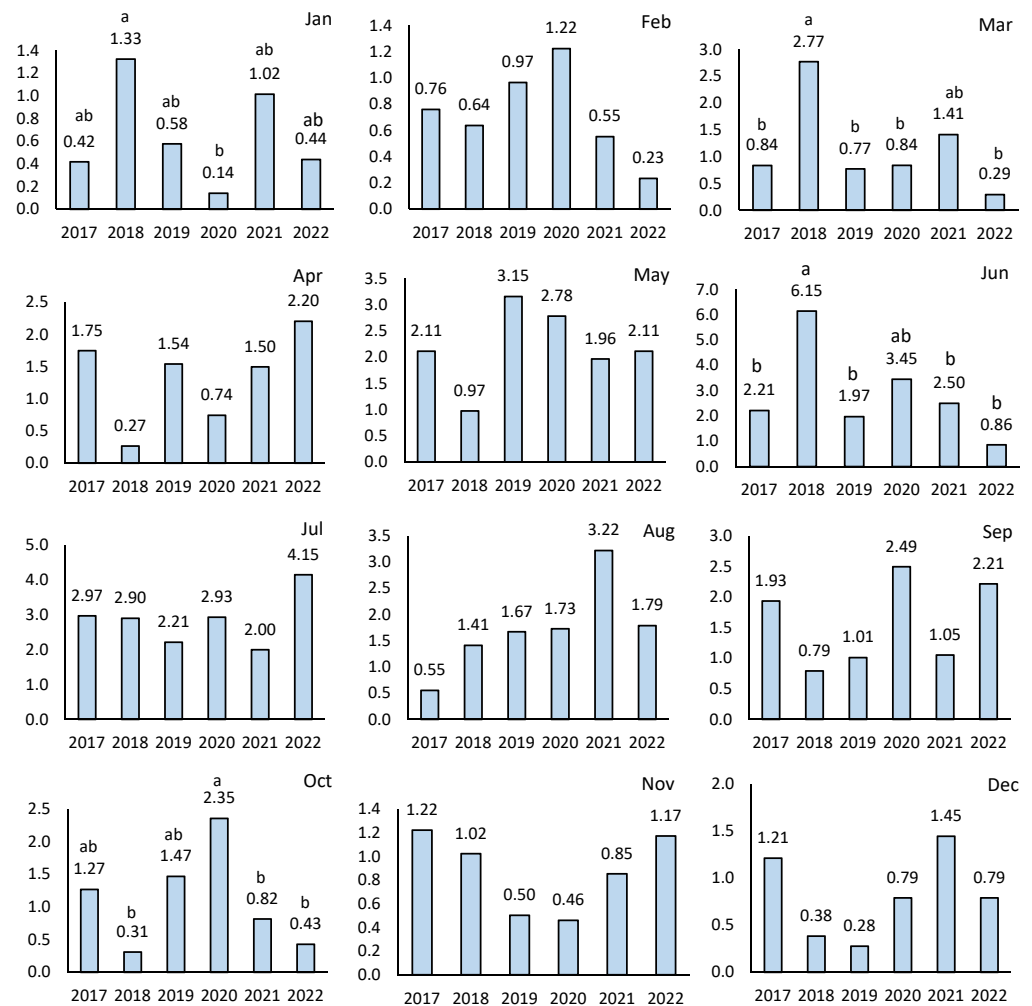


**Figure 8.** The average daily precipitation changes by month from 2017 to 2022. (Different letters indicate statistically significant differences ( $p \leq 0.05$ )).

The findings revealed that the temperature in June 2022 increased significantly (at the 5% level) when compared to 2021 and 2020. In addition, when the average temperatures of different months were compared from 2017 to 2022, it was found that it significantly decreased (at the 5% level) in the first month of autumn (September) in 2021 (Figure 9). Early autumn is the time for terminal bud formation and nutrient storage for the following year’s growth.

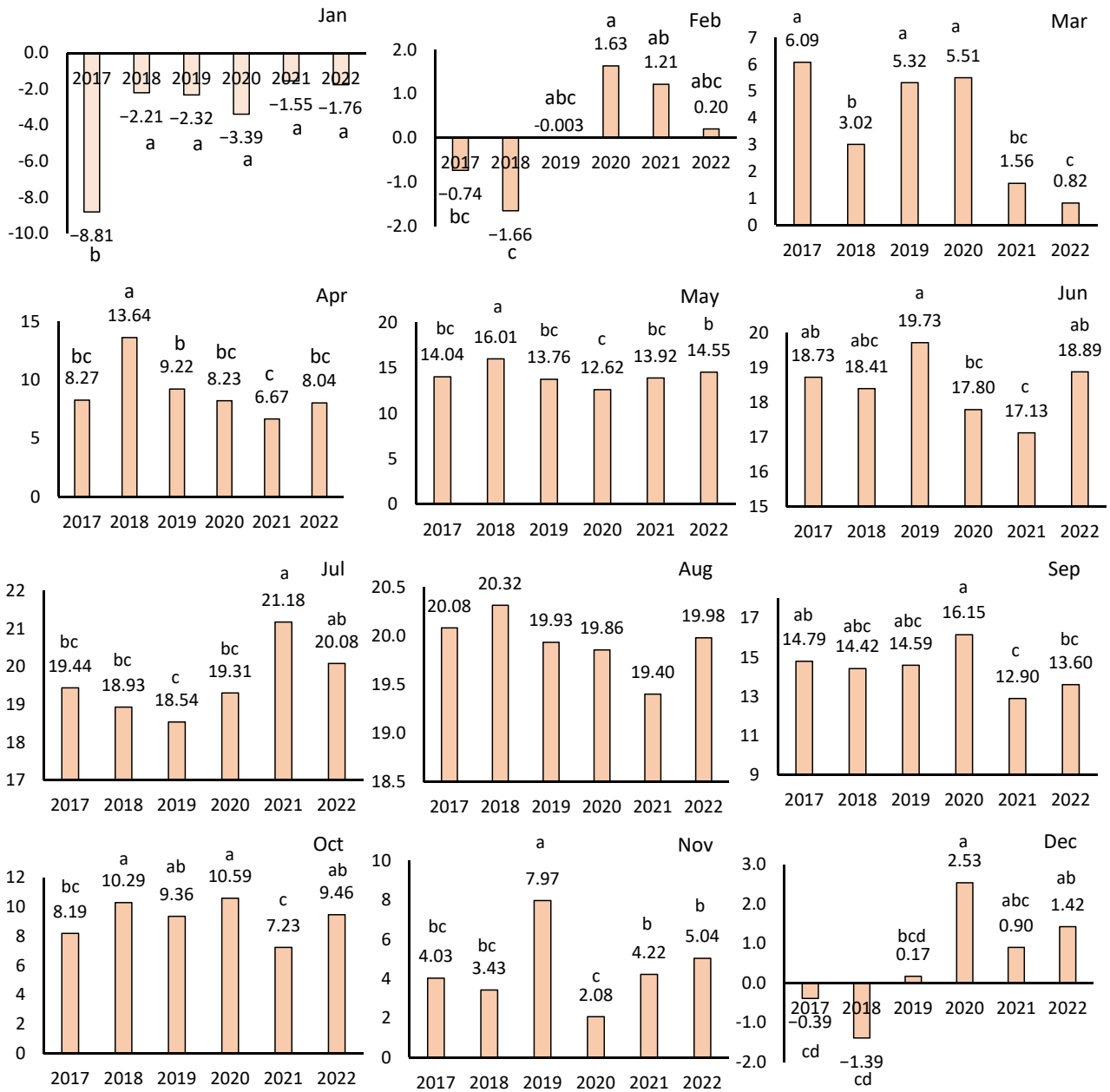


**Figure 9.** The average daily temperature changes by month from 2017 to 2022. (Different letters indicate statistically significant differences ( $p \leq 0.05$ )).

The results of correlation analysis, which depict the monthly variations in NDVI, precipitation, and temperature, are shown in Figure 10. According to the findings, there is a strong and significant (at the 1% level) positive correlation between NDVI, precipitation ( $r = 0.527$ ), and temperature ( $r = 0.883$ ), respectively.

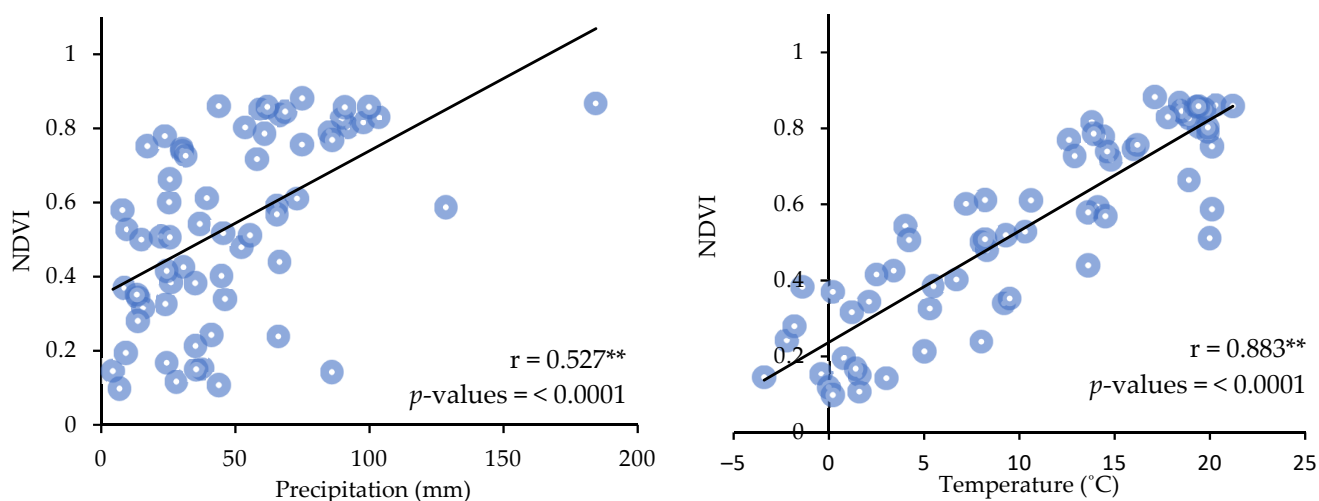


**Figure 10.** Pearson correlation ( $r$ ) results between NDVI, rainfall, and temperature from 2017 to 2022. (\*\*: statistically significant at the 1% level).

#### 4. Discussion

Mapping agricultural use is important for identifying crops, analyzing crops and cropping systems' spatial distribution, and recording land cover trends in different areas. As the world's climate changes, this becomes increasingly important [66]. In this context, it is critical to develop proper procedures for accelerating such investigations. The simultaneous use of Google Maps and PlanetScope satellite images, as well as Sentinel-2 images and multispectral instruments with 13 bands for image classification, to prepare ground-truth samples was an appropriate strategy for identifying and detecting willow crops in the study area, with high accuracy (more than 98%) demonstrated for all six maps created between 2017 and 2022. In fact, the rate of accuracy achieved in this study exceeds the average rates obtained with hyperspace images using object-based classification algorithms [77,78]. Kpienbaareh et al. [79] found that using Sentinel-2 and PlanetScope data to produce maps of agricultural regions in Sub-Saharan Africa improved the accuracy of land cover maps by more than 85%. Mercie et al. [63] and Gašparović and Jogun [80] reported similar findings and indicated that production maps are very accurate when Sentinel-2 is integrated with PlanetScope for vegetation mapping and monitoring. Nomura and Mitchard's [47] research also used Sentinel-2 data to classify a complex mosaic of different land uses in a forest ecosystem, as well as using WorldView-3 and UAV images to create ground-truth samples. The classification of 13 Sentinel-2 bands using the random forest classification approach yielded an overall accuracy of more than 95%. Due to a lack of data and information regarding the willow-farmed land in Romania, as well as the relatively small ownership of such agricultural systems, the use of such techniques in the research area may provide a good opportunity for future studies.

The NDVI was used to evaluate the health of willow crops. The application of the NDVI has aided remote sensing applications since it is connected to the state of a wide variety of plant properties. Remote sensing has transformed how humans see, use, and manage Earth's resources [81]. The same is true for how the NDVI is associated with vegetation characteristics (e.g., health, patterns, and status). Coops and Stone [82] and McVeagh et al. [83] have shown that for local-scale vegetation management, the NDVI is employed as a direct measure of vegetation health and growth. The findings of this study indicated that the value for this index in 2022 was much lower than in previous years (i.e., 2017 to 2021). Since the NDVI mostly varies due to changes in environmental conditions (precipitation and temperature) [69], meteorological data on temperature and precipitation were used to assess the cause of this index's decline in 2022. The plant growth season in Europe begins at the end of May and lasts until the end of October. Precipitation data analysis found that the rainfall in June had decreased substantially in 2022. The decrease in

rainfall of this month appears to have resulted in a decrease in mass growth for a plant like a willow, which is a hydrophile. According to these findings, NDVI index data derived from Sentinel-2 satellite images offer a high potential for precise monitoring of agricultural stages based on the crop calendar. Liberacki et al. [84] studied willow demands for water during their vegetation season in western Poland and found that this species needed 402 to 408 mm of water on average throughout the growth season. In this regard, June's 0.85 cm (=8.5 mm) of precipitation was too low to support plant development.

The analysis of average temperature changes from 2017 to 2022, on the other hand, shows that the average temperature has risen in recent years. This increase in temperature across the growing seasons creates short-term droughts, which have a direct impact on crop growth [85]. Hao et al. [86] reported that the NDVI reacted more strongly at higher temperatures. According to global forecasts, temperatures will continue to increase and precipitation will decrease, requiring preventative actions in Romania to deal with the negative implications of water shortages during the growing season [87]. Willows do not require strict cultivation conditions, according to researchers [88]. Mirck and Volk [89] report that willows can resist irrigation with water containing 1625 mg of chlorine. In addition, they reported that willows are only modestly salt tolerant. Based on these findings, it is possible to conclude that the willow can adapt to some extent. It should be noted that proper watering of willows is required for their best growth. According to Gage and Cooper [90], one of the decisive factors for willow development in mountain and coastal communities in the United States of America is the availability of water in the soil.

Decisions on what crops can be used in place of fossil fuels should be made in such a way that they do not considerably increase water demand [91]. Research is increasingly being conducted to simulate agricultural water demands and the amount of irrigation water required under various climate change scenarios [92,93]. According to previous estimations, climate change has an impact on the amount of water required for irrigation. Climate change will also increase the need for irrigation for several crops [94].

## 5. Conclusions

This study focused on mapping the extent of willow-cultivated land in a complex agricultural area using a combination of medium and high spatial resolution satellite images. The approach to mapping was generally robust throughout the study area, with the capacity to map willow and non-willow plots with varying features. Sentinel-2 and PlanetScope images provided important data, while the dot-grid photo interpretation approach, based on the random forest classification method, was well translated throughout the region, allowing willow-cultivated plots to be accurately identified. However, the classification of satellite images in the study area revealed a decreasing trend in willow cultivation. In addition to the spatiotemporal changes in willow crops, understanding their health status is critical for the proper management of these systems. The NDVI was used in this study to assess the health status of the willow crops, and it experienced a decreasing trend. Most likely, this is due to the changing patterns in the quantity of precipitation and the temperature in the area of study. The use of additional remote sensing vegetation indices and climate variables will need to be studied more in the future so as to improve our ability to accurately classify willow plots and to understand the changes that are occurring in these agricultural systems.

**Author Contributions:** H.B.H.: conceptualization, data curation, formal analysis, investigation, methodology, software, roles/writing—original draft. O.O.-S.: data curation, formal analysis, investigation. M.V.M.: data curation, investigation, resources. S.A.B.: conceptualization, investigation, project administration, supervision, validation, writing—review and editing. All authors have read and agreed to the published version of the manuscript.

**Funding:** This research received no external funding.

**Data Availability Statement:** Data supporting this study may be provided by the first author upon a reasonable request. The data are not publicly available due to privacy of parts of the data.

**Acknowledgments:** Hadi Beygi Heidarlou’s research at the Transilvania University of Brasov, Romania, has been supported by the program “Transilvania Fellowship for Postdoctoral Research/Young Researchers”. The authors would like to thank to Vahid Nasiri, University of Agriculture in Krakow, Poland, for his support. We would like to thank the Planet team for providing us high temporal and spatial resolution satellite images.

**Conflicts of Interest:** The authors declare no conflicts of interest.

## References

1. Kowalczyk, Z.; Kwaśniewski, D. Environmental impact of the cultivation of energy willow in Poland. *Sci. Rep.* **2021**, *11*, 1–15.
2. Fischer, G.; Schrattenholzer, L. Global bioenergy potentials through 2050. *Biomass Bioenergy* **2001**, *20*, 151–159. [[CrossRef](#)]
3. Kopetz, H. Build a biomass energy market. *Nature* **2013**, *494*, 29–31. [[CrossRef](#)]
4. Murphy, F.; Devlin, G.; McDonnell, K. Energy requirements and environmental impacts associated with the production of short rotation willow (*Salix* sp.) chip in Ireland. *GCB Bioenergy* **2014**, *6*, 727–739. [[CrossRef](#)]
5. Scriba, C.; Borz, S.; Talagai, N. Estimating dry mass and bark proportion in one-year shoots yielded by one-year *Salix viminalis* L. plantations in Central Romania. *Rev. Pădur.* **2014**, *129*, 57–66.
6. Borz, S.A.; Nita, M.D.; Talagai, N.; Scriba, C.; Grigolato, S.; Proto, A.R. Performance of small-scale technology in planting and cutback operations of short-rotation willow crops. *Trans. ASABE* **2019**, *62*, 167–176. [[CrossRef](#)]
7. Ozdogan, M. The spatial distribution of crop types from MODIS data: Temporal unmixing using Independent Component Analysis. *Remote Sens. Environ.* **2010**, *114*, 1190–1204. [[CrossRef](#)]
8. Liu, X.; Zhai, H.; Shen, Y.; Lou, B.; Jiang, C.; Li, T.; Hussain, S.B.; Shen, G. Large-scale crop mapping from multisource remote sensing images in google earth engine. *IEEE J. Sel. Top. Appl. Earth Obs. Remote Sens.* **2020**, *13*, 414–427. [[CrossRef](#)]
9. Hansen, M.C.; Potapov, P.V.; Moore, R.; Hancher, M.; Turubanova, S.A.; Tyukavina, A.; Thau, D.; Stehman, S.V.; Goetz, S.J.; Loveland, T.R. High-resolution global maps of 21st-century forest cover change. *Science* **2013**, *342*, 850–853. [[CrossRef](#)]
10. Zarin, D.J.; Harris, N.L.; Baccini, A.; Aksenov, D.; Hansen, M.C.; Azevedo-Ramos, C.; Azevedo, T.; Margono, B.A.; Alencar, A.C.; Gabris, C. Can carbon emissions from tropical deforestation drop by 50% in 5 years? *Glob. Biol.* **2016**, *22*, 1336–1347. [[CrossRef](#)]
11. Till, N. From Reference Levels to Results Reporting: REDD+ under the UNFCCC. *For. Clim. Chang. Work. Pap.* **2017**, *15*. [[CrossRef](#)]
12. Gibbs, H.K.; Ruesch, A.S.; Achard, F.; Clayton, M.K.; Holmgren, P.; Ramankutty, N.; Foley, J.A. Tropical forests were the primary sources of new agricultural land in the 1980s and 1990s. *Proc. Natl. Acad. Sci. USA* **2010**, *107*, 16732–16737. [[CrossRef](#)]
13. Di Tommaso, S.; Wang, S.; Lobell, D.B. Combining GEDI and Sentinel-2 for wall-to-wall mapping of tall and short crops. *Environ. Res. Lett.* **2021**, *16*, 125002. [[CrossRef](#)]
14. Calderón-Loor, M.; Hadjikakou, M.; Bryan, B.A. High-resolution wall-to-wall land-cover mapping and land change assessment for Australia from 1985 to 2015. *Remote Sens. Environ.* **2021**, *252*, 112148. [[CrossRef](#)]
15. Zemin, L.; Zong, W. Image classification optimization algorithm based on SVM. *J. Multimed.* **2013**, *8*, 496–502.
16. Lowder, S.K.; Skoet, J.; Raney, T. The number, size, and distribution of farms, smallholder farms, and family farms worldwide. *World Dev.* **2016**, *87*, 16–29. [[CrossRef](#)]
17. Masters, W.A.; Djurfeldt, A.A.; De Haan, C.; Hazell, P.; Jayne, T.; Jirström, M.; Reardon, T. Urbanization and farm size in Asia and Africa: Implications for food security and agricultural research. *Glob. Food Secur.* **2013**, *2*, 156–165. [[CrossRef](#)]
18. Georganos, S.; Grippa, T.; Vanhuyse, S.; Lennert, M.; Shimoni, M.; Kalogirou, S.; Wolff, E. Less is more: Optimizing classification performance through feature selection in a very-high-resolution remote sensing object-based urban application. *GISci. Remote Sens.* **2018**, *55*, 221–242. [[CrossRef](#)]
19. Aljahdali, M.O.; Munawar, S.; Khan, W.R. Monitoring mangrove forest degradation and regeneration: Landsat time series analysis of moisture and vegetation indices at Rabigh Lagoon, Red Sea. *Forests* **2021**, *12*, 52. [[CrossRef](#)]
20. Kogan, F.N. Remote sensing of weather impacts on vegetation in non-homogeneous areas. *Int. J. Remote Sens.* **1990**, *11*, 1405–1419. [[CrossRef](#)]
21. Rhyma, P.; Norizah, K.; Hamdan, O.; Faridah-Hanum, I.; Zulfa, A. Integration of normalised different vegetation index and Soil-Adjusted Vegetation Index for mangrove vegetation delineation. *Remote Sens. Appl. Soc. Environ.* **2020**, *17*, 100280. [[CrossRef](#)]
22. Clevers, J.G.; Kooistra, L.; Van den Brande, M.M. Using Sentinel-2 data for retrieving LAI and leaf and canopy chlorophyll content of a potato crop. *Remote Sens.* **2017**, *9*, 405. [[CrossRef](#)]
23. de Jong, R.; Verbesselt, J.; Schaepman, M.E.; De Bruin, S. Trend changes in global greening and browning: Contribution of short-term trends to longer-term change. *Glob. Chang. Biol.* **2012**, *18*, 642–655. [[CrossRef](#)]
24. Chen, F.; Bai, X.; Liu, F.; Luo, G.; Tian, Y.; Qin, L.; Li, Y.; Xu, Y.; Wang, J.; Wu, L. Analysis long-term and spatial changes of forest cover in typical karst areas of China. *Land* **2022**, *11*, 1349. [[CrossRef](#)]
25. Madson, A.; Dimson, M.; Fortini, L.B.; Kawelo, K.; Ticktin, T.; Keir, M.; Dong, C.; Ma, Z.; Beilman, D.W.; Kay, K. A near four-decade time series shows the Hawaiian Islands have been browning since the 1980s. *Environ. Manag.* **2023**, *71*, 965–980. [[CrossRef](#)] [[PubMed](#)]
26. Vuorinne, I.; Heiskanen, J.; Pellikka, P.K. Assessing leaf biomass of agave sisalana using sentinel-2 vegetation indices. *Remote Sens.* **2021**, *13*, 233. [[CrossRef](#)]

27. Tucker, C.J. Red and photographic infrared linear combinations for monitoring vegetation. *Remote Sens. Environ.* **1979**, *8*, 127–150. [[CrossRef](#)]
28. Hmimina, G.; Dufrêne, E.; Pontailleur, J.-Y.; Delpierre, N.; Aubinet, M.; Caquet, B.; De Grandcourt, A.; Burban, B.; Flechard, C.; Granier, A. Evaluation of the potential of MODIS satellite data to predict vegetation phenology in different biomes: An investigation using ground-based NDVI measurements. *Remote Sens. Environ.* **2013**, *132*, 145–158. [[CrossRef](#)]
29. Cai, Z.; Jönsson, P.; Jin, H.; Eklundh, L. Performance of smoothing methods for reconstructing NDVI time-series and estimating vegetation phenology from MODIS data. *Remote Sens.* **2017**, *9*, 1271. [[CrossRef](#)]
30. Verhoeven, V.B.; Dedoussi, I.C. Annual satellite-based NDVI-derived land cover of Europe for 2001–2019. *J. Environ. Manag.* **2022**, *302*, 113917. [[CrossRef](#)] [[PubMed](#)]
31. Ramanath, A.; Muthusrinivasan, S.; Xie, Y.; Shekhar, S.; Ramachandra, B. Ndvi versus cnn features in deep learning for land cover clasification of aerial images. In Proceedings of the IGARSS 2019—2019 IEEE International Geoscience and Remote Sensing Symposium, Yokohama, Japan, 28 July–2 August 2019; pp. 6483–6486.
32. Jiang, L.; Liu, Y.; Wu, S.; Yang, C. Analyzing ecological environment change and associated driving factors in China based on NDVI time series data. *Ecol. Indic.* **2021**, *129*, 107933. [[CrossRef](#)]
33. Nanzad, L.; Zhang, J.; Tuvdendorj, B.; Nabil, M.; Zhang, S.; Bai, Y. NDVI anomaly for drought monitoring and its correlation with climate factors over Mongolia from 2000 to 2016. *J. Arid Environ.* **2019**, *164*, 69–77. [[CrossRef](#)]
34. Lawley, V.; Lewis, M.; Clarke, K.; Ostendorf, B. Site-based and remote sensing methods for monitoring indicators of vegetation condition: An Australian review. *Ecol. Indic.* **2016**, *60*, 1273–1283. [[CrossRef](#)]
35. Leon, J.R.R.; Van Leeuwen, W.J.; Casady, G.M. Using MODIS-NDVI for the modeling of post-wildfire vegetation response as a function of environmental conditions and pre-fire restoration treatments. *Remote Sens.* **2012**, *4*, 598–621. [[CrossRef](#)]
36. Talagai, N.; Marcu, M.V.; Zimbalatti, G.; Proto, A.R.; Borz, S.A. Productivity in partly mechanized planting operations of willow short rotation coppice. *Biomass Bioenergy* **2020**, *138*, 105609. [[CrossRef](#)]
37. Dimitriou, I.; Mola-Yudego, B. Poplar and willow plantations on agricultural land in Sweden: Area, yield, groundwater quality and soil organic carbon. *For. Ecol. Manag.* **2017**, *383*, 99–107. [[CrossRef](#)]
38. Choudhury, M.R.; Christopher, J.; Das, S.; Apan, A.; Menzies, N.W.; Chapman, S.; Mellor, V.; Dang, Y.P. Detection of calcium, magnesium, and chlorophyll variations of wheat genotypes on sodic soils using hyperspectral red edge parameters. *Environ. Technol. Innov.* **2022**, *27*, 102469. [[CrossRef](#)]
39. Zhang, H.; Li, J.; Liu, Q.; Lin, S.; Huete, A.; Liu, L.; Croft, H.; Clevers, J.G.; Zeng, Y.; Wang, X. A novel red-edge spectral index for retrieving the leaf chlorophyll content. *Methods Ecol. Evol.* **2022**, *13*, 2771–2787. [[CrossRef](#)]
40. Holzman, M.E.; Rivas, R.E.; Bayala, M.I. Relationship between TIR and NIR-SWIR as indicator of vegetation water availability. *Remote Sens.* **2021**, *13*, 3371. [[CrossRef](#)]
41. Chong, L.; Liu, H.-J.; Lu, L.-P.; Liu, Z.-R.; Kong, F.-C.; Zhang, X.-L. Monthly composites from Sentinel-1 and Sentinel-2 images for regional major crop mapping with Google Earth Engine. *J. Integr. Agric.* **2021**, *20*, 1944–1957.
42. Clevers, J.G.; Gitelson, A.A. Remote estimation of crop and grass chlorophyll and nitrogen content using red-edge bands on Sentinel-2 and-3. *Int. J. Appl. Earth Obs. Geoinf.* **2013**, *23*, 344–351. [[CrossRef](#)]
43. Marta, S. *Planet Imagery Product Specifications*; Planet Labs: San Francisco, CA, USA, 2018; Volume 91.
44. Shendryk, Y.; Rist, Y.; Ticehurst, C.; Thorburn, P. Deep learning for multi-modal classification of cloud, shadow and land cover scenes in PlanetScope and Sentinel-2 imagery. *ISPRS J. Photogramm. Remote Sens.* **2019**, *157*, 124–136. [[CrossRef](#)]
45. Barrett, J.P.; Philbrook, J.S. Dot grid area estimates: Precision by repeated trials. *J. For.* **1970**, *68*, 149–151.
46. Bonnor, G. The error of area estimates from dot grids. *Can. J. For. Res.* **1975**, *5*, 10–17. [[CrossRef](#)]
47. Nomura, K.; Mitchard, E.T. More than meets the eye: Using Sentinel-2 to map small plantations in complex forest landscapes. *Remote Sens.* **2018**, *10*, 1693. [[CrossRef](#)]
48. Beygi Heidarlou, H.; Banj Shafiei, A.; Nasiri, V.; Niță, M.D.; Borz, S.A.; Lopez-Carr, D. Impact of Iran’s Forest Nationalization Law on Forest Cover Changes over Six Decades: A Case Study of a Zagros Sparse Coppice Oak Forest. *Sensors* **2023**, *23*, 871. [[CrossRef](#)]
49. Schulz, D.; Yin, H.; Tischbein, B.; Verleysdonk, S.; Adamou, R.; Kumar, N. Land use mapping using Sentinel-1 and Sentinel-2 time series in a heterogeneous landscape in Niger, Sahel. *ISPRS J. Photogramm. Remote Sens.* **2021**, *178*, 97–111. [[CrossRef](#)]
50. Breiman, L. *Random Forests—Random Features, Technical Report 567*; Statistics Department, University of California: Berkeley, CA, USA, 1999.
51. Lee, J.S.H.; Wich, S.; Widayati, A.; Koh, L.P. Detecting industrial oil palm plantations on Landsat images with Google Earth Engine. *Remote Sens. Appl. Soc. Environ.* **2016**, *4*, 219–224. [[CrossRef](#)]
52. Pal, M.; Mather, P. Some issues in the classification of DAIS hyperspectral data. *Int. J. Remote Sens.* **2006**, *27*, 2895–2916. [[CrossRef](#)]
53. Thenkabail, P.S.; Enclona, E.A.; Ashton, M.S.; Van Der Meer, B. Accuracy assessments of hyperspectral waveband performance for vegetation analysis applications. *Remote Sens. Environ.* **2004**, *91*, 354–376. [[CrossRef](#)]
54. Le Bris, A.; Chehata, N.; Briottet, X.; Paparoditis, N. Spectral band selection for urban material classification using hyperspectral libraries. In Proceedings of the 23 ISPRS Congress, International Society for Photogrammetry and Remote Sensing (ISPRS), Prague, Czech Republic, 12–19 July 2016; pp. 33–40.
55. da Silva, V.S.; Salami, G.; da Silva, M.I.O.; Silva, E.A.; Monteiro Junior, J.J.; Alba, E. Methodological evaluation of vegetation indexes in land use and land cover (LULC) classification. *Geol. Ecol. Landsc.* **2020**, *4*, 159–169. [[CrossRef](#)]

56. Rouse, R.A. Conformational analysis of saturated heterocycles substituted final ozonides. *Int. J. Quantum Chem.* **1973**, *7*, 289–294. [CrossRef]
57. Martín-Sotoca, J.J.; Saa-Requejo, A.; Moratiel, R.; Dalezios, N.; Faraslis, I.; Tarquis, A.M. Statistical analysis for satellite-index-based insurance to define damaged pasture thresholds. *Nat. Hazards Earth Syst. Sci.* **2019**, *19*, 1685–1702. [CrossRef]
58. Gitelson, A.A.; Merzlyak, M.N. Remote sensing of chlorophyll concentration in higher plant leaves. *Adv. Space Res.* **1998**, *22*, 689–692. [CrossRef]
59. Qi, J.; Chehbouni, A.; Huete, A.R.; Kerr, Y.H.; Sorooshian, S. A modified soil adjusted vegetation index. *Remote Sens. Environ.* **1994**, *48*, 119–126. [CrossRef]
60. Huete, A.; Didan, K.; Miura, T.; Rodriguez, E.P.; Gao, X.; Ferreira, L.G. Overview of the radiometric and biophysical performance of the MODIS vegetation indices. *Remote Sens. Environ.* **2002**, *83*, 195–213. [CrossRef]
61. Pizarro, S.E.; Pricope, N.G.; Vargas-Machuca, D.; Huanca, O.; Ñaupari, J. Mapping Land Cover Types for Highland Andean Ecosystems in Peru Using Google Earth Engine. *Remote Sens.* **2022**, *14*, 1562. [CrossRef]
62. Baumann, M.; Radeloff, V.C.; Avedian, V.; Kuemmerle, T. Land-use change in the Caucasus during and after the Nagorno-Karabakh conflict. *Reg. Environ. Chang.* **2015**, *15*, 1703–1716. [CrossRef]
63. Mercier, A.; Betbeder, J.; Rumiano, F.; Baudry, J.; Gond, V.; Blanc, L.; Bourgoin, C.; Cornu, G.; Ciudad, C.; Marchamalo, M. Evaluation of Sentinel-1 and 2 time series for land cover classification of forest–agriculture mosaics in temperate and tropical landscapes. *Remote Sens.* **2019**, *11*, 979. [CrossRef]
64. Kpienbaareh, D.; Sun, X.; Wang, J.; Luginaah, I.; Bezner Kerr, R.; Lupafya, E.; Dakishoni, L. Crop type and land cover mapping in northern Malawi using the integration of sentinel-1, sentinel-2, and planetscope satellite data. *Remote Sens.* **2021**, *13*, 700. [CrossRef]
65. Lillesand, T.; Kiefer, R.W.; Chipman, J. *Remote Sensing and Image Interpretation*; John Wiley & Sons: Hoboken, NJ, USA, 2015.
66. Zhou, C.; Ou, Y.; Ma, T.; QIN, B. Theoretical perspectives of CA-based geographical system modeling. *Prog. Geogr.* **2009**, *28*, 833–838.
67. Li, T.; Wang, Y.; Liu, C.; Tu, S. Research on identification of multiple cropping index of farmland and regional optimization scheme in China based on NDVI data. *Land* **2021**, *10*, 861. [CrossRef]
68. Deng, S.; Gao, M.; Ren, C.; Li, S.; Liang, Y. Extraction of Sugarcane Planting Area Based on Similarity of NDVI Time Series. *IEEE Access* **2022**, *10*, 117362–117373. [CrossRef]
69. Ghebregabher, M.G.; Yang, T.; Yang, X.; Sereke, T.E. Assessment of NDVI variations in responses to climate change in the Horn of Africa. *Egypt. J. Remote Sens. Space Sci.* **2020**, *23*, 249–261. [CrossRef]
70. Prăvălie, R.; Sîrodoev, I.; Nita, I.-A.; Patriche, C.; Dumitraşcu, M.; Roşca, B.; Tişcovschi, A.; Băndoc, G.; Săvulescu, I.; Mănoiu, V. NDVI-based ecological dynamics of forest vegetation and its relationship to climate change in Romania during 1987–2018. *Ecol. Indic.* **2022**, *136*, 108629. [CrossRef]
71. Stamford, J.D.; Violet-Chabrand, S.; Cameron, I.; Lawson, T. Development of an accurate low cost NDVI imaging system for assessing plant health. *Plant Methods* **2023**, *19*, 9. [CrossRef] [PubMed]
72. Ienco, D.; Interdonato, R.; Gaetano, R.; Minh, D.H.T. Combining Sentinel-1 and Sentinel-2 Satellite Image Time Series for land cover mapping via a multi-source deep learning architecture. *ISPRS J. Photogramm. Remote Sens.* **2019**, *158*, 11–22. [CrossRef]
73. Nowak, B.; Marliac, G.; Michaud, A. Estimation of winter soil cover by vegetation before spring-sown crops for mainland France using multispectral satellite imagery. *Environ. Res. Lett.* **2021**, *16*, 064024. [CrossRef]
74. ESA. Level-1C Cloud Masks-Sentinel-2 MSI Technical Guide-Sentinel Online. Available online: <https://sentinel.esa.int/web/sentinel/technical-guides/sentinel-2-msi/level-1c/cloud-masks> (accessed on 8 May 2023).
75. GEE. Landsat Algorithms in Google Earth Engine API. Available online: <https://developers.google.com/earth-engine/landsat> (accessed on 8 May 2023).
76. Gärtner, P. How Cloudy Is My Sentinel-2 Image Collection?—The ‘QA60’ Band Gives Insights. Available online: <https://philippgaertner.github.io/2020/08/percent-cloud-cover/> (accessed on 14 August 2020).
77. Amini, S.; Homayouni, S.; Safari, A.; Darvishsefat, A.A. Object-based classification of hyperspectral data using Random Forest algorithm. *Geo-Spat. Inf. Sci.* **2018**, *21*, 127–138. [CrossRef]
78. Su, T.; Zhang, S. Local and global evaluation for remote sensing image segmentation. *ISPRS J. Photogramm. Remote Sens.* **2017**, *130*, 256–276. [CrossRef]
79. Kpienbaareh, D.; Mohammed, K.; Luginaah, I.; Wang, J.; Bezner Kerr, R.; Lupafya, E.; Dakishoni, L. Estimating Groundnut Yield in Smallholder Agriculture Systems Using PlanetScope Data. *Land* **2022**, *11*, 1752. [CrossRef]
80. Gašparović, M.; Jogun, T. The effect of fusing Sentinel-2 bands on land-cover classification. *Int. J. Remote Sens.* **2018**, *39*, 822–841. [CrossRef]
81. Huang, S.; Tang, L.; Hupy, J.P.; Wang, Y.; Shao, G. A commentary review on the use of normalized difference vegetation index (NDVI) in the era of popular remote sensing. *J. For. Res.* **2021**, *32*, 1–6. [CrossRef]
82. Coops, N.C.; Stone, C. A comparison of field-based and modelled reflectance spectra from damaged *Pinus radiata* foliage. *Aust. J. Bot.* **2005**, *53*, 417–429. [CrossRef]
83. McVeagh, P.; Yule, I.; Grafton, M. Pasture yield mapping from your groundspread truck. In *Advanced Nutrient Management: Gains from the Past-Goals for the Future*; Fertilizer and Lime Research Centre: Palmerston North, New Zealand, 2012.

84. Liberacki, D.; Kocięcka, J.; Stachowski, P.; Rolbiecki, R.; Rolbiecki, S.; Sadan, H.A.; Figas, A.; Jagosz, B.; Wichrowska, D.; Ptach, W. Water Needs of Willow (*Salix L.*) in Western Poland. *Energies* **2022**, *15*, 484. [[CrossRef](#)]
85. Szwed, M.; Karg, G.; Pińskwar, I.; Radziejewski, M.; Graczyk, D.; Kędziora, A.; Kundzewicz, Z. Climate change and its effect on agriculture, water resources and human health sectors in Poland. *Nat. Hazards Earth Syst. Sci.* **2010**, *10*, 1725–1737. [[CrossRef](#)]
86. Hao, F.; Zhang, X.; Ouyang, W.; Skidmore, A.K.; Toxopeus, A. Vegetation NDVI linked to temperature and precipitation in the upper catchments of Yellow River. *Environ. Model. Assess.* **2012**, *17*, 389–398. [[CrossRef](#)]
87. Kocur-Bera, K.; Rapiński, J.; Siejka, M.; Leń, P.; Małek, A. Potential of an Area in Terms of Pro-Climate Solutions in a Land Consolidation Project. *Sustainability* **2023**, *15*, 9306. [[CrossRef](#)]
88. Mirck, J.; Zalesny, R.S. Mini-review of knowledge gaps in salt tolerance of plants applied to willows and poplars. *Int. J. Phytoremediat.* **2015**, *17*, 640–650. [[CrossRef](#)] [[PubMed](#)]
89. Mirck, J.; Volk, T.A. Response of three shrub willow varieties (*Salix* spp.) to storm water treatments with different concentrations of salts. *Bioresour. Technol.* **2010**, *101*, 3484–3492. [[CrossRef](#)] [[PubMed](#)]
90. Gage, E.A.; Cooper, D.J. Constraints on willow seedling survival in a Rocky Mountain montane floodplain. *Wetlands* **2004**, *24*, 908–911. [[CrossRef](#)]
91. Pierzgałski, E.; Mańk, K. Energy crops in aspect of water resources in Poland. In *Agro-Energy for Sustainable Agriculture and Rural Development*; Slovak University of Agriculture in Nitra: Nitra-Chrenová, Slovakia, 2016; p. 50.
92. Ewaid, S.H.; Abed, S.A.; Al-Ansari, N. Crop water requirements and irrigation schedules for some major crops in Southern Iraq. *Water* **2019**, *11*, 756. [[CrossRef](#)]
93. Zhang, Y.; Wang, Y.; Niu, H. Effects of temperature, precipitation and carbon dioxide concentrations on the requirements for crop irrigation water in China under future climate scenarios. *Sci. Total Environ.* **2019**, *656*, 373–387. [[CrossRef](#)]
94. Masia, S.; Trabucco, A.; Spano, D.; Snyder, R.L.; Sušnik, J.; Marras, S. A modelling platform for climate change impact on local and regional crop water requirements. *Agric. Water Manag.* **2021**, *255*, 107005. [[CrossRef](#)]

**Disclaimer/Publisher’s Note:** The statements, opinions and data contained in all publications are solely those of the individual author(s) and contributor(s) and not of MDPI and/or the editor(s). MDPI and/or the editor(s) disclaim responsibility for any injury to people or property resulting from any ideas, methods, instructions or products referred to in the content.